CONEM 2016 CONGRESSO NACIONAL DE ENGENHARIA MECÂNICA
21 - 25 AGOSTO DE 2016 FORTALEZA - CEARÁ
ABCM 40 anos Associação Brasileira de Engenharia e Ciências Mecânicas

CONTROL OF ROTORDYNAMIC SYSTEM USING SHAPE MEMORY ALLOYS

Marina Castro dos Santos, marinacastsant@poli.ufrj.br[1]
Marcelo A. Savi, savi@mecanica.coppe.ufrj.br[1]
Marco Tulio Santana Alves, mtalves@hotmail.com[2]
Ilmar F. Santos, ifs@mek.dtu.dk[3]
Valder Steffen Jr., vssteffen@ufu.br[2]

[1]Universidade Federal do Rio de Janeiro, COPPE - Department of Mechanical Engineering, Center for Nonlinear Mechanics 21.941.972 - Rio de Janeiro - RJ - Brazil, P.O. Box 68.503
[2]Technical University of Denmark, Department of Mechanical Engineering, DK -2800 Kgs. Lyngby, Denmark
[3]Federal University of Uberlândia, School of Mechanical Engineering, Av. João Naves de Ávila, 2121, Uberlândia, MG, 38408-196, Brazil

Abstract: *Shape memory alloys (SMAs) exhibit solid-phase transformations and have remarkable properties that are interesting when considering dynamical applications. Temperature dependence and hysteretic behavior may be exploited in order to perform control of rotordynamic systems. This paper investigates adaptive-passive control applied to a horizontal flexible unbalanced rotor. SMA wires are coupled to bearings providing the adaptive behavior induced by temperature variations. Experimental and numerical approaches are employed in order to analyze the lateral vibration of the rotor. Temperature variations are exploited to eliminate undesirable behaviors, reducing vibration amplitudes. The experimental test rig has exhibited a satisfactory response with adaptive-passive control reducing vibration levels. Temperature variations modify critical speed of the rotor system, reducing vibration amplitudes.*
Keywords: *SMA, passive control, smart materials, nonlinear dynamics, rotordynamics*

1. INTRODUCTION

Rotordynamic is an essential part of machine mechanics representing the main rotating components of motors or machines which spin about their axis, such as drive shafts. Nowadays, one of the main challenges in engineering rotor design is to increase the operational speed whilst remaining stable and maintaining efficiency. One of the most important concerns is the vibration associated with ‘critical speeds’, i.e., the rotational speed at which resonance of the system occurs. Control forces are usually employed to deal with dynamical responses of the rotor at the critical speed, preventing damages. Damping effects are also exploited but is usually associated with the expend of energy. In order to try and achieve a proper control using less energy than classical control techniques, several control systems have been developed. Some of these alternatives employ smart materials that have adaptive behavior due to a coupling between different physical fields. Basically, the idea is to change dynamical characteristics due to variation of some external field as electric, magnetic or temperature.

Among smart materials, shape memory alloys (SMAs) constitute one of the candidates to be employed in rotordynamic systems. These alloys provide solid phase transformations induced either by stress or by temperature, which can help to produce adaptive behavior of the rotor system. In brief, SMAs have two cristalographic phases: martensite and austenite. Austenitic phase is stable at high temperatures in a stress-free state. On the other hand, martensitic phase is stable at low temperatures in a stress-free state. Besides, martensite present variants that are induced by stress fields. Macroscopically speaking, an SMA presents hysteretic behavior and two essential phenomena are important to be highlighted: pseudoelasticity and shape memory effect. Based on these remarkable properties, SMAs can be employed to build rotor suspensions, providing a kind of adaptive-passive control. Various research teams around the world are trying to exploit this idea in different ways.

Nagaya *et al.* (1987) used SMA springs attached to a rotor bearing with antagonistic actuation based on thermal actuation. Simulations are carried out considering a uniform shaft with discs and also a stepped shaft without disc. Thermal loadings of the SMA spring were provided by Joule effect, where a fine nichrome wire is wound around the SMA spring. Enemark *et al.* (2015) introduced SMA elements on a vertical rotor that also used magnetic bearings. The main idea was to compare results of bearing using steel and SMA at different temperatures showing the adaptive behavior of SMA system. Results showed that critical speed behaviors are avoided with temperature variations.

A different approach is related to the use of SMA in order to dissipate energy during impacts between shaft and bearing.Silva *et al.* (2013) analyzed a Jeffcott rotor comparing results of the classical bearing, with elastic supports, and an SMA bearing. Numerical results showed that less critical behaviors are induced by SMA support and it is possible to control the response using temperature variations.

The present paper deals with the use of SMA elements to design a rotor system with adaptive-passive control. The experimental apparatus is designed to analyze a flexible unbalanced rotor using SMA wires attached to the bearing. The control is carried out by temperature variations provided by a heating chamber. The influence of temperature variations on system response is analyzed showing that the undesirable behaviors of the rotor can be avoided. A model based on the finite element method is implemented Alves *et al.* (2015). SMA effect is restricted to the bearing and the thermomechanical description is performed using a variation of the Brinson's constitutive model. A comparison between experimental and numerical results is performed, verifying the general aspects of the model. Results show that the use of SMA-bearing can successfully reduce vibration with temperature variations, avoiding undesirable responses.

2. EXPERIMENTAL APPARATUS

An SMA experimental apparatus designed by Alves (2015) is employed to investigate the use of SMA elements on rotordynamical systems. The experimental test rig is shown in Figure1 and the schematic picture of the rotor is shown in Figure2a. Note that the rotor system is composed by a flexible shaft [4] with an unbalanced disc [5]. The shaft is connected to an electric motor [1] by a flexible coupling [3], and supported by two ball bearings [2]-[6]. The details of the bearings close to the chamber are presented in Figure 2c and Figure 2b. The SMA-bearing employs SMA wires [4] in a structure that has lateral supports [1], heat guns [2] and a heat chamber [3].

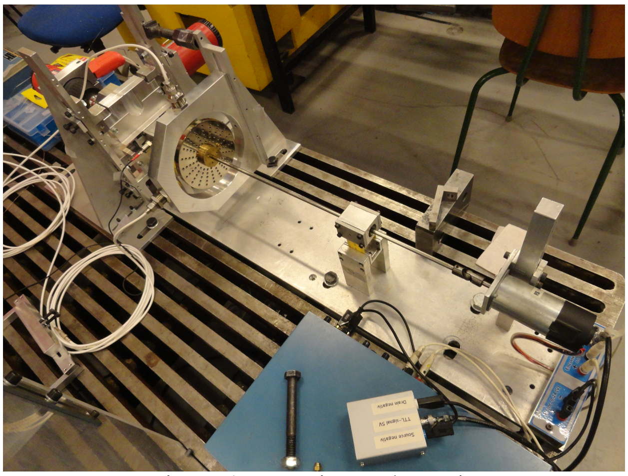

Figura 1: Experimental test rig

Figures 2b and 2c present details about the SMA-bearings. SMA wires are employed in such a way that phase transformations are induce due to rotor system vibrations. Pseudoelastic behavior is of concern and therefore, hysteretic temperature dependent response is expected, leading to energy dissipation. Wires need to be pre-stressed in order to either avoid compressive response or to control the amount of dissipation related to the hysteresis loop. A heat chamber controls the temperature.

3. NUMERICAL MODELS

Numerical simulations are performed considering a rotor system model build with the aid of the finite element method. A two node element with eight degrees of freedom is employed considering two displacements and two rotations per node.

The SMA-bearing considers the SMA element acting as a boundary condition. The global model considers a discretization of 17 elements as illustrated in Figure 3. Besides, the unbalanced mass is located 25 mm from the center of the disc and it is equal to 1.8g.

The SMA-rotor system is monitored by different sensors that include an encoder, two proximity sensors, an accelerometer and two thermocouples.

On this basis, the global equation of motion can be written as follows:

$$\boldsymbol{M}^s\ddot{\boldsymbol{q}}^s + \boldsymbol{D}^s\dot{\boldsymbol{q}}^s + \boldsymbol{K}^s\boldsymbol{q}^s = \boldsymbol{Q}^s \qquad (1)$$

where $\mathbf{M}$ is the mass matrix of the rotor coupled discs and bearings; $\mathbf{D}^s$=-(Ω $\mathbf{G}^s$- $\mathbf{C}^s$); Ω is the angular velocity of the rotor; $\mathbf{G}^s$ is the gyroscopic matrix; $\mathbf{C}^s$ is the matrix of damping coefficients of the rotor; and $\mathbf{K}$ is the stiffness matrix of the rotor coupled discs and bearings.

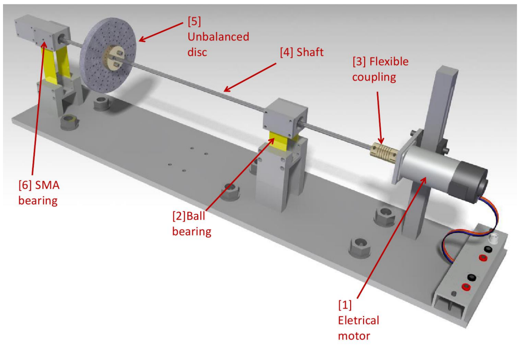

(a) Schematics of the test rig

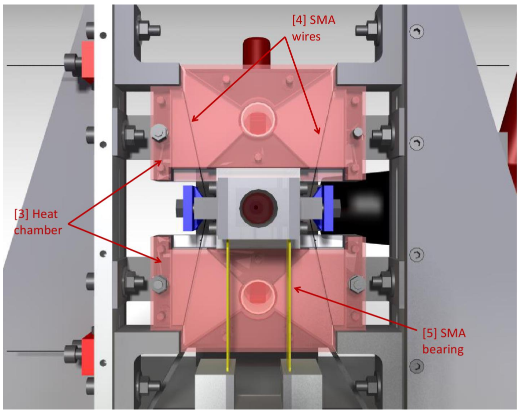

(b) Schematics of the SMA wires coupled to the SMA bearing.

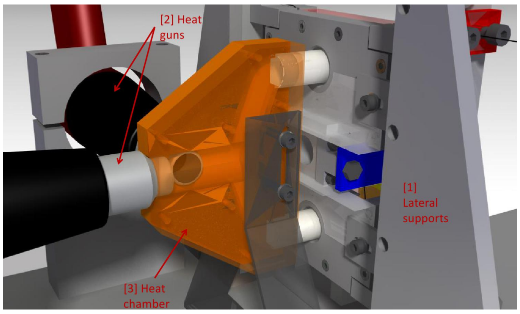

(c) Schematics of the Heat chamber with focus at the heat guns.

Figura 2: SMA rotor.

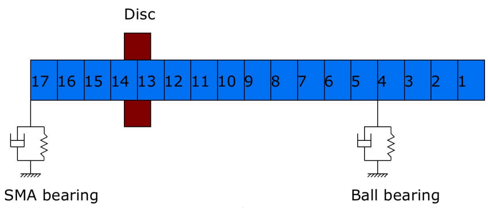

Figura 3: Finite element mesh of the rotor coupled to SMA wires.

The thermomechanical description of the SMA element needs to be presented with a proper constitutive model, as shown in the next section.

3.1 SMA constitutive model

The rotor bearing with SMA elements exhibits nonlinear behavior provided by solid phase transformations. Here, pseudoelastic behavior is of concern considering an SMA sample at high temperature, where the austenitic phase is stable in a stress-free state. Under this condition, when a stress field is applied, phase transformation from austenite to martensite is induced during stress loading. During unloading, a reverse transformation from martensite to austenite occurs.

The thermomechanical description of SMAs can be performed by different ways. Paiva and Savi (2006) and Hartl and Lagoudas (2008) presented a general overview of the constitutive modeling of SMAs. Here, the model due to Brinson is employed (Brinson, 1993; Brinson and Huang,1996 and Bekker and Brinson,1998). Essentially, the model assumes a martensitic volume fraction that is split into a stress induced part, ξ_S, and into a temperature induced part, ξ_T,

$$\xi = \xi_S + \xi_T \tag{2}$$

Since only pseudoelastic behavior is important for the experimental application, it is possible to neglect temperature induced volume fraction. The constitutive model is described by the following equation:

$$\sigma - \sigma_0 = D(\xi)\epsilon - D(\xi_0)\epsilon_0 + \Omega(\xi)\xi_s - \Omega(\xi_0)\xi_{s0} + \theta(T - T_0) \tag{3}$$

where $D(\epsilon, \xi, T)$ is a function representative of the modulus of the SMA material, $\Omega(\epsilon, \xi, T)$ is the transformation tensor, $\theta(\epsilon, \xi, T)$ is a function related to the thermal coefficient of expansion for the SMA material and $(\sigma_0, \epsilon_0, \xi_0, T_0)$ represents the initial state (or initial conditions) of the material. Under these assumptions, constitutive equation can be written as follows:

$$\sigma = E(\epsilon - \epsilon_L \xi) \tag{4}$$

where σ is the axial stress and ϵ is the strain. Besides, $E = E_A + \xi(E_M - E_A)$, where E_M and E_A are respectively, the Young's modulii of martensite and austenite, and ϵ_L is the residual strain due to phase transformation.

The volume fraction evolution is defined as a function of temperature T and stress σ, presented in the sequence.

- If $\dot{\sigma} - C_A\dot{T} > 0$ and $\sigma_{M_s} \leq \sigma \leq \sigma_{A_s}$ then
  $X_f = \frac{\sigma - \sigma_{M_s}}{\sigma_{M_f} - \sigma_{M_s}}$

$$f_f = f(X_f) \tag{5}$$

$$\xi = \xi_0 + (1 - \xi_0) f_f \tag{6}$$

Reverse transformation from detwinned martensite to austenite is given by:

- If $\dot{\sigma} - C_M\dot{T} < 0$ and $\sigma_{A_f} \leq \sigma \leq \sigma_{A_s}$ then
  $X_r = \frac{\sigma - \sigma_{A_f}}{\sigma_{A_s} - \sigma_{A_f}}$

$$f_r = f(X_r) \tag{7}$$

$$\xi = \xi_0 + f_r \tag{8}$$

Note that phase transformation critical stress values are given by:
$\sigma_{M_s} = C_M(T - M_s)$, $\sigma_{M_f} = C_M(T - M_f)$
$\sigma_{A_s} = C_A(T - A_s)$, $\sigma = C_A(T - A_f)$
where M_s and M_f are the temperature of start and finish of martensitic phase transformations; A_s and A_f are the temperature of start and finish of austenitic phase transformations; C_A and C_M are the slopes of austenite and martensite formation.

Bekker and Brinson (1998) proposed a cosine function as the hardening function for *forward* and *reverse* tranformations. In the present work, a cubic Bézier curve proposed by Alves *et al.* (2015) is employed. According to Alves *et al.* (2015), the cubic Bézier curve ensures genuine smoothness (infinite differentiability) to the process considered. The Bézier curve $\mathbf{B}$ is designated by the points $(0, 0)$, $(n_1, 0)$, $(1 - n_2, 1)$ and $(1, 1)$, which results in the following parametric representation:

$$\mathbf{B(s)} = \begin{Bmatrix} B_x(s) \\ B_y(s) \end{Bmatrix} = \begin{Bmatrix} (3n_1 + 3n_2 - 2)s^3 - 3(2n_1 + n_2 - 1)s^2 + 3n_1 s \\ -2s^3 + 3s^2 \end{Bmatrix} \tag{9}$$

Parameters n_1, $n_2 \in (0;1)$ control the curvature of the function and their values are defined from experimental data. Therefore, $(n_1, n_2)_f$ and $(n_1, n_2)_r$ respectively represent the controlling parameters for the forward and reverse transformations. Based on that, the hardening functions can be expressed as follows:

$$f(x) = B_y(s) \mid B_x(s) = x, \; for \; x \in [0;1] \tag{10}$$

Figure 4 shows a comparison between some Bézier curves and those using cosine functions (Alves *et al.* (2015)). For more details about the use of cubic Bézier curves to represent hardening functions, please see Enemark and Santos (2015). Typical model parameters employed in this paper for SMA wires are presented in Table 1.

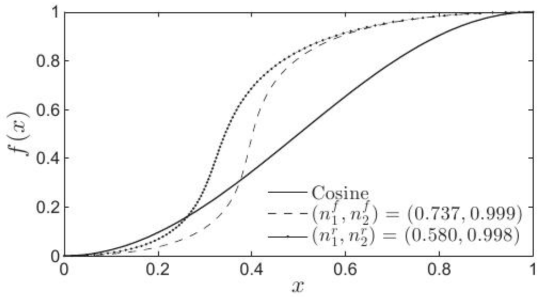

Figura 4: Hardening functions in the forward and reverse transformations Alves *et al.* (2015).

Tabela 1: Parameters used in the wire model using the Brinson model with smooth hardening.

$\epsilon_L[\%]$	$E_A[GPa]$	$E_M[GPa]$	$A_s[°C]$	$A_f[°C]$	$M_s[°C]$	$M_f[°C]$	$C_A[\frac{MPa}{°C}]$	$C_M[\frac{MPa}{°C}]$	${n_1}^f$	${n_2}^f$	${n_1}^r$	${n_2}^r$
4.08	42.9	27.1	−25.3	30.0	25.0	−49.1	8.03	9.32	0.737	0.999	0.580	0.998

3.2 Rotor-Bearing Forces

Based on constitutive equations, it is possible to evaluate the effect of SMA wires on the bearing. Geometric considerations are also important to establish the generated forces. Figure 5 presents the general aspect of the SMA-bearing, highlighting the SMA elements. Initial and deformed configurations are presented. The SMA-bearing uses pre-stressed SMA elements.

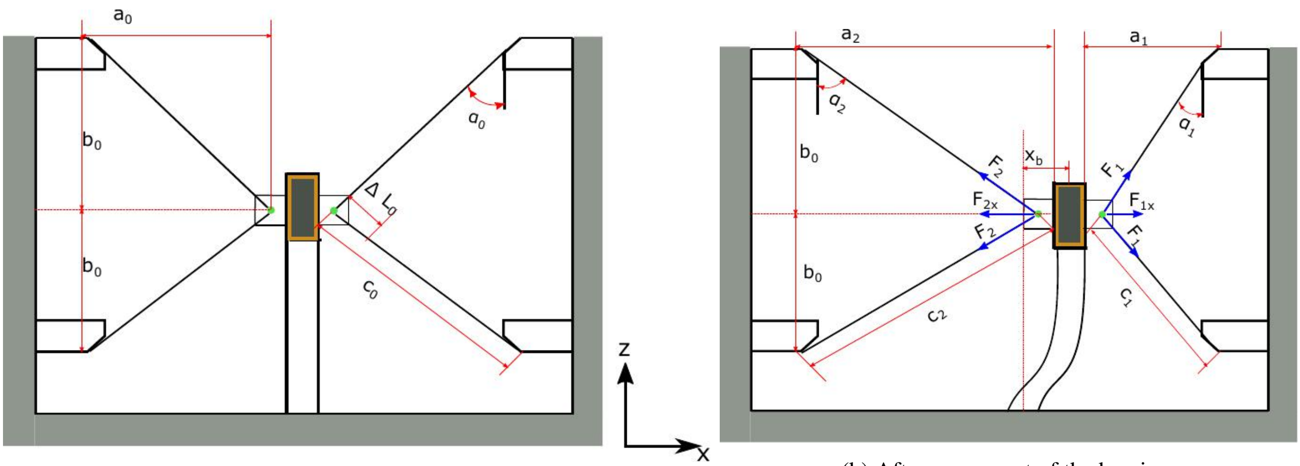

(a) Pre tension state.

(b) After movement of the bearing.

Figura 5: (a) and (b) Schematic of the SMA Wire Elongation System.

Based on both configurations, the following definitions should be done:

ΔL_0: elongation of the wire in a pre-tensioned state.

$b0 = L$: relaxed length of the wire (half of the total wire, due to the symmetry)

$c_0 = L + \Delta L_0$: length of the wire in a pre-tensioned state - rotor at time-out.

It is important to emphasize that this SMA system only acts along the x-axis, and the wires work as nonlinear springs. The SMA wires are Nickel-Titanium alloy (NiTi) with 160mm lenght and 0.25mm diameter.

Based on the geometry illustrated in Figure 5 and on the definition of strain as $\epsilon_0 = \frac{(c_0 - b_0)}{b_0} = \frac{\Delta L_0}{L}$, the following equation can be deduced:

$$c_1^2 = a_1^2 + b_0^2 = (a_0 - x_b)^2 + L^2 = x_b^2 - 2a_0 x_b + \underbrace{L^2 + a_0^2}_{c_0^2} \tag{11}$$

Resulting in the relation,

$$c_1 = \sqrt{x_b^2 - 2x_b L(1+\epsilon_0)\sin\alpha_0 + [L(1+\epsilon_0)]^2} \tag{12}$$

Analogous relation can be obtained for c_2:

$$c_2 = \sqrt{x_b^2 + 2x_b L(1+\epsilon_0)\sin\alpha_0 + [L(1+\epsilon_0)]^2} \tag{13}$$

These equations can be rewritten using the strain definition:

$$\epsilon_1 = \frac{\sqrt{x_b^2 - 2x_b L(1+\epsilon_0)\sin\alpha_0 + [(1+\epsilon_0)L]^2 - L}}{L} \tag{14}$$

and

$$\epsilon_2 = \frac{\sqrt{x_b^2 + 2x_b L(1+\epsilon_0)\sin\alpha_0 + [(1+\epsilon_0)L]^2 - L}}{L} \tag{15}$$

The forces acting on the wires in the x direction are shown in Figure 5b and be obtained assuming that $F = \sigma A$ where σ is the stress evaluated from the constitutive model and A is the cross sectional area,

$$F_{1x} = 2F_1 \sin\alpha_1 = 2F_1 \left(\frac{a_1}{c_1}\right) \tag{16}$$

$$F_{1x} = \frac{2\sigma_1 A[L(1+\epsilon_0)\sin\alpha_0 - x_b]}{\sqrt{x_b^2 - 2x_b L(1+\epsilon_0)\sin\alpha_0 + [(1+\epsilon_0)L]^2}} \tag{17}$$

where force F_1 pulls the SMA bearing along one direction and force F_2 does the same in the opposite direction. Consequently, F_2 can be defined as follows:

$$F_{2x} = \frac{2\sigma_2 A[L(1+\epsilon_0)\sin\alpha_0 + x_b]}{\sqrt{x_b^2 + 2x_b L(1+\epsilon_0)\sin\alpha_0 + [(1+\epsilon_0)L]^2}} \tag{18}$$

Hence, the total force applied by the wire elongation system to the SMA bearing is defined as $F_{SMA} = F_{1x} - F_{2x}$.

4. RESULTS

This section presents an analysis of results obtained from both experimental and numerical approaches. Qualitative comparisons between these two approaches are performed, verifying the general aspects of the model. The main goal is the use of temperature variation for vibration reduction.

4.1 Experimental Results

The rotordynamic system is evaluated considering run-up tests for three different temperatures: 30^oC, 45^oC and 60^oC. Essentially, frequency is changed from $0 - 30Hz$ with a variation rate of $1Hz/s$. Figure 6 illustrates frequency variations, temperature evolution, and displacements along the x direction and z direction, for the SMA-bearing. In addition, the displacement versus frequency curve is also shown. It can be observed that temperature variation changes the critical speed. Note that, considering a frequency of $18.76Hz$, temperature change can decrease the vibration amplitude from 25.4% to 32.4%, considering the temperature changes adopted (30^oC to 45^oC and 30^oC to 60^oC).

4.2 Numerical Results

Numerical simulations consider the same general conditions of the experimental tests. Initially, run-up tests are determined for different temperatures. Figure 8 shows the unbalance response obtained from a linear run-up profile for three different temperatures. In general, numerical results are qualitatively coherent with experimental data. By considering the critical speed of $17.32Hz$, it is possible to observe that temperature variations decrease vibration amplitude from 2.3% to 8.2%.

Hysteretic behavior can be investigated from the model by evaluating the force-displacement curves. Figure 10a presents the force-displacement hysteric curve of the SMA-bearing. Note that temperature variation alters the average stiffness of the SMA, also changing the hysteresis behavior. This change leads to an influence on the disc orbits as shown in Figure 10b. The area of the SMA force-displacement curve increases 1% as temperature varies from 30^oC to 45^oC and this area increases 2% for variations from 30^oC to 60^oC.

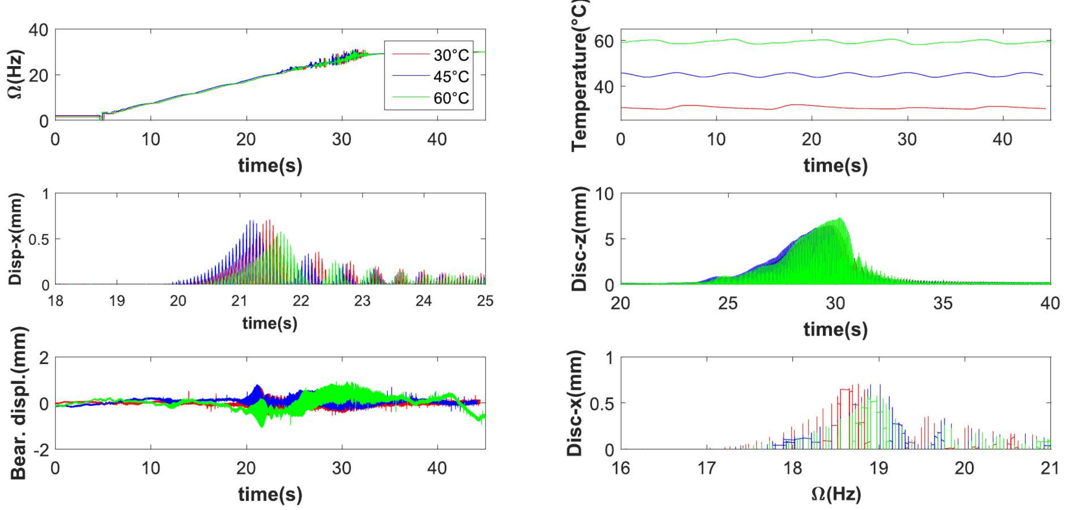

(a) Run-up curve, temperature, disc displacement in horizontal direction, disc displacement in vertical direction, bearing displacement as a function of frequency.

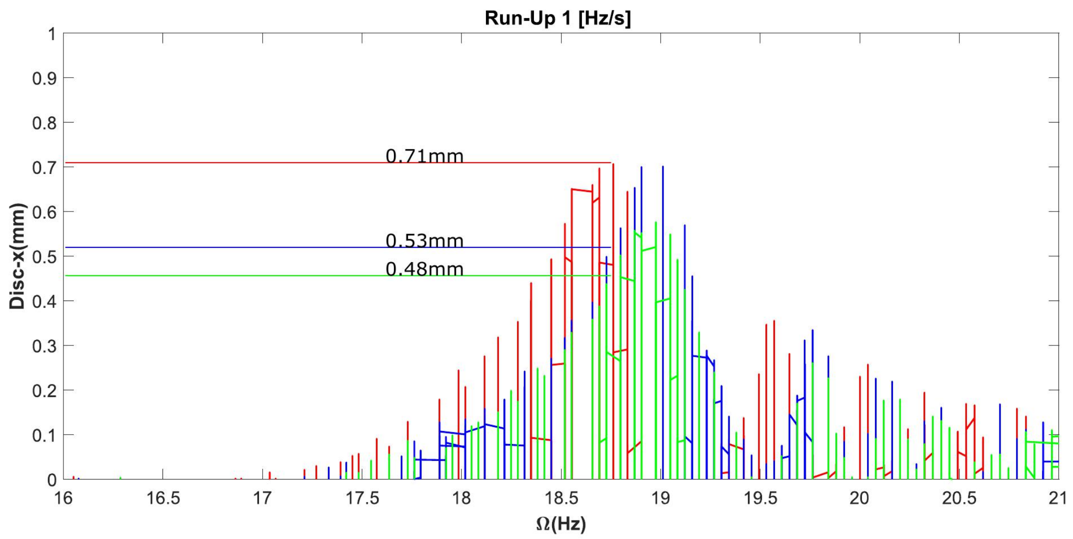

(b) Displacement as function of frequency of the disc along the x direction

Figura 6: Experimental results.

Figure 7 presents the vibration response considering the rotor operating at three different rotation speeds and three temperatures. Note that the vibration amplitude at the first critical speed decreases from 15% to 30% considering the temperature changes adopted (30^oC to 45^oC and 30^oC to 60^oC).

5. CONCLUSIONS

This paper deals with an investigation of the use of SMAs on rotor systems. An SMA-bearing is developed producing an adaptive behavior that can alter system response due to temperature variations. Numerical and experimental results are evaluated, showing a qualitative agreement. Experimental test rig has exhibited a satisfactory response as an adaptive-passive control, reducing vibration levels. Temperature variations modify the rotor critical speed allowing vibration amplitude reduction. This characteristic can be used as a smart mechanism for crossing critical speeds. New geometries of the SMA-bearing can be designed providing a more effective influence of the SMA element, increasing the control capacity for vibration reduction.

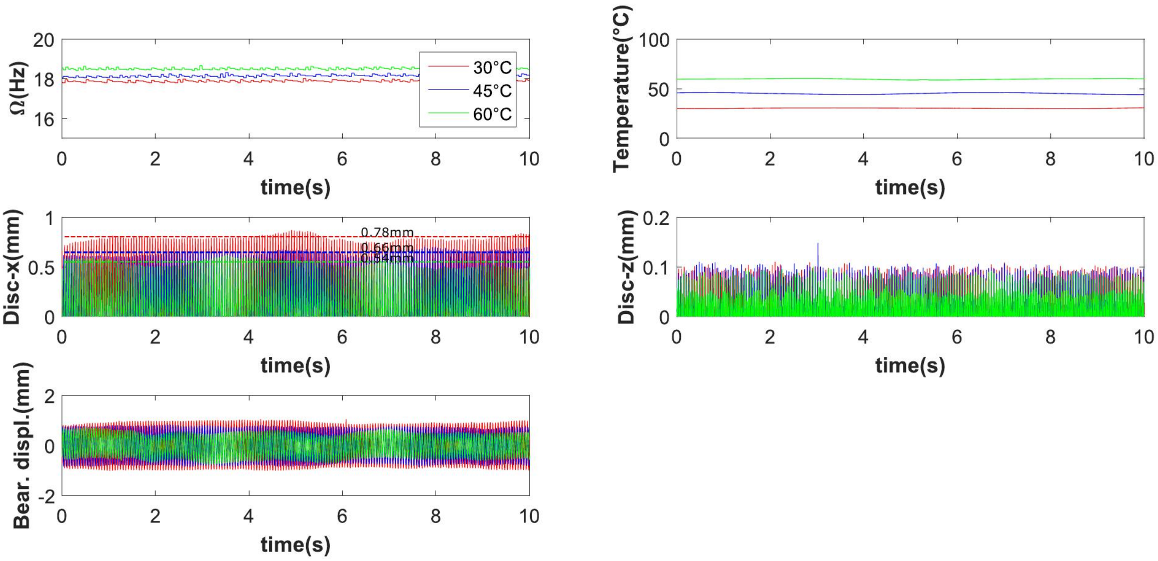

Figura 7: Experimental results at the critical speed.

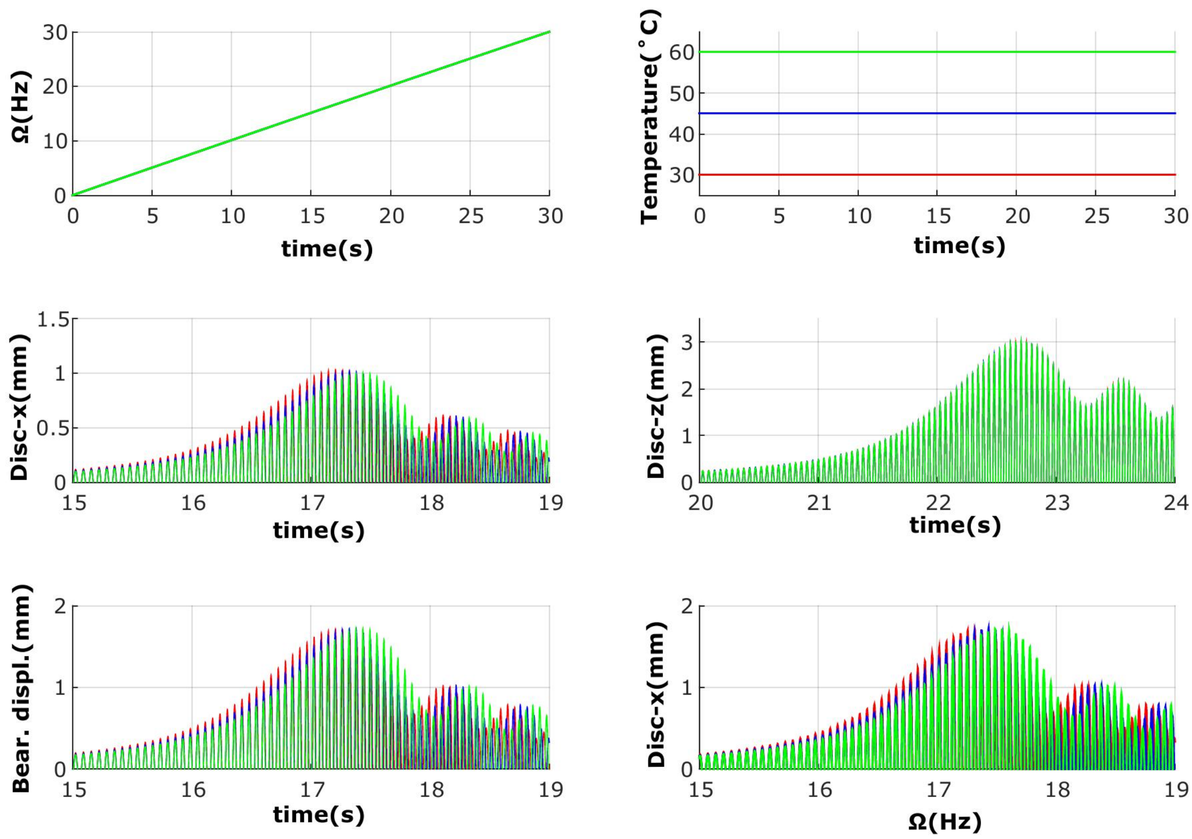

Figura 8: Run-up and temperature curves.

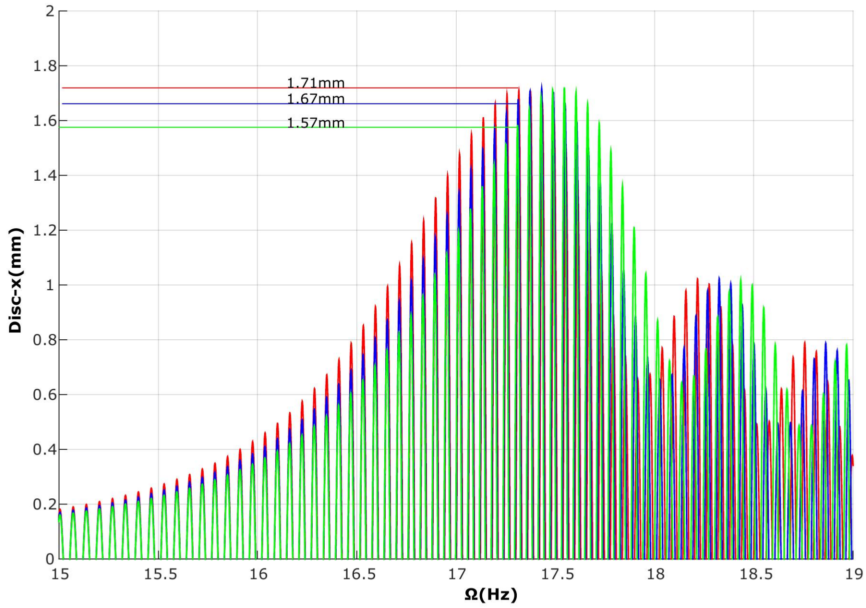

Figura 9: Unbalance response obtained along the x direction at the disc position.

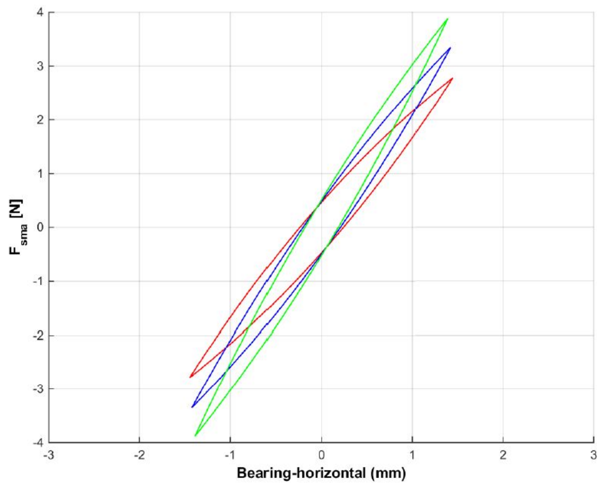

(a) Numerical simulation of the wire force by bearing displacement.

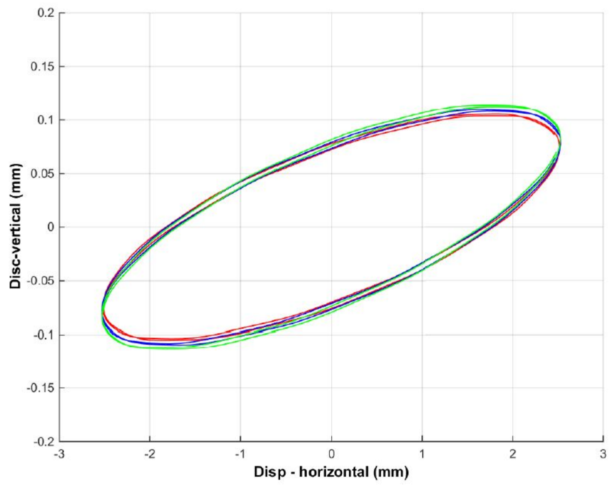

(b) Orbit of vertical displacement of the disc by horizontal displacement of the disc.

Figura 10: Numerical results.

6. ACKNOWLEDGEMENTS

The authors would like to acknowledge the support of the Brazilian Research Agencies CNPq, CAPES and FAPERJ and through the INCT-EIE (National Institute of Science and Technology - Smart Structures in Engineering) the CNPq and FAPEMIG. The Air Force Office of Scientific Research (AFOSR) is also acknowledged. Besides, Technical University of Denmark supported by FTP research project (12-127502) should also be mentioned.

7. REFERENCES

Alves, M., 2015. *Vibration Control of Rotating Machinery using Shape Memory Alloys (PhD Thesis - in Portuguese)*. Universidade Federal de Uberlândia.

Alves, M.T.S., Enemark, S., Steffen Jr, V. and Santos, I., 2015. "Vibration control of a flexible rotor using shape memory alloy wires". In *Proceedings of the 17th International Symposium on Dynamic Problems of Mechanics*.

Bekker, A. and Brinson, L., 1998. "Phase diagram based description of the hysteresis behavior of shape memory alloys". *Acta materialia*, Vol. 46, No. 10, pp. 3649–3665.

Brinson, L., 1993. "One-dimensional constitutive behavior of shape memory alloys: thermomechanical derivation with non-constant material functions and redefined martensite internal variable". *Journal of intelligent material systems and structures*, Vol. 4, No. 2, pp. 229–242.

Brinson, L. and Huang, M., 1996. "Simplifications and comparisons of shape memory alloy constitutive models". *Journal of intelligent material systems and structures*, Vol. 7, No. 1, pp. 108–114.

Enemark, S. and Santos, I.F., 2015. "Quasi-static characterisation of trained pseudoelastic shape memory alloy wire subjected to cyclic loading: transformation kinetics". *Journal of Intelligent Material Systems and Structures*, p. 1045389X15585900.

Enemark, S., Santos, I.F. and Savi, M.A., 2015. "Shape memory alloys applied to improve rotor-bearing system dynamics– an experimental investigation".

Hartl, D. and Lagoudas, D., 2008. *Thermomechanical characterization of shape memory alloy materials*. Springer.

Nagaya, K., Takeda, S., Tsukui, Y. and Kumaido, T., 1987. "Active control method for passing through critical speeds of rotating shafts by changing stiffnesses of the supports with use of memory metals". *Journal of Sound and Vibration*, Vol. 113, No. 2, pp. 307–315.

Paiva, A. and Savi, M.A., 2006. "An overview of constitutive models for shape memory alloys". *Mathematical Problems in Engineering*, Vol. 2006.

Silva, L.C., Savi, M.A. and Paiva, A., 2013. "Nonlinear dynamics of a rotordynamic nonsmooth shape memory alloy system". *Journal of Sound and Vibration*, Vol. 332, No. 3, pp. 608–621.

8. AUTHORIAL RESPONSIBILITY

The authors are the only responsible for the content of this work.